Conformational Flexibility of L-Alanine Zwitterion Determines Shapes of Raman and Raman Optical Activity Spectral Bands

Josef Kapitán,[†,‡] Vladimír Baumruk,*[,‡] Vladimír Kopecký, Jr.,[‡] and Petr Bouř*[,†]

Institute of Organic Chemistry and Biochemistry, Academy of Sciences, Flemingovo nám. 2, 16610, Prague, Czech Republic, and Charles University, Faculty of Mathematics and Physics, Institute of Physics, Ke Karlovu 5, 12116, Prague, Czech Republic

Received: January 13, 2006; In Final Form: January 31, 2006

Detailed analysis of Raman and Raman optical activity (ROA) of L-alanine zwitterion (ALAZW) revealed that shapes of the spectral bands are to a large extent determined by the rotation of the NH_3^+, CO_2^-, and CH_3 groups. Aqueous solution ALAZW spectra were measured down to 100 cm^{-1} and compared to complex simulations based on ab initio (B3LYP/CPCM/6-31++G**) computations of molecular energies and spectral parameters. The bands exhibit different sensitivities to the motion of the rotating group; typically, for more susceptible bands the Raman signal becomes broader and the ROA intensity decreases. When these dynamical factors are taken into account in Boltzmann averaging of conformer contributions, simulated spectra not only better agree with the experiment, but shapes of the rotational potentials can be estimated. Effects of the molecular flexibility could be also demonstrated on differences in Raman spectra of the solution, crystalline, and glass (gellike) solid states of ALAZW. Experimental Raman and ROA spectra of four model dipeptides of different rigidities (Ala-Pro, Pro-Ala, Pro-Gly, and Gly-Pro) indicate that the broadening of spectral lines can be used as a general site-specific indicator of molecular rigidity or flexibility.

Introduction

The vast area of applications of molecular manipulations in medicine, chemical synthesis, and industry fuels ongoing interest in fundamental molecular properties and interactions governing molecular dynamics in different media. Advances of the computational techniques based on first principles[1] enabled better involvement of the molecular environment including the solvent[2−6] and allowed for modeling of finer structural details. This provides an important feedback into spectroscopic techniques, such as those exploring the Raman scattering, interpretation of which is to a large extent dependent on solid theoretical models.[7] In this study, we concentrate ourselves on a particular problem, flexibility and dynamics of the three rotating molecular residues in L-alanine zwitterion, as such motions seem to be crucial for correct interpretation of the Raman and Raman optical activity (ROA) spectra. It is generally accepted that the inhomogeneous line width broadening of spectral lines is caused by equilibria of many conformations and solvent interactions.[8−12] In the past many studies were dedicated to resolution of conformational mixtures by vibrational spectroscopy.[13−16] Yet the movement of the CH_3, NH_3, and CO_2 groups has been traditionally considered only as a side-product of solvent clustering.[16,17] However, for L-alanine, we can demonstrate that this motion significantly contributes to the formation of spectral shapes. In fact, experimental profiles cannot be explained unless the conformational averaging is taken into account. This is in agreement with surface,[18] glass, and crystalline solid-state (this paper) alanine spectra that exhibit much narrower bands. Experimental spectra of dipeptide molecules brought up in the discussion additionally suggest that the band-broadening phenomena may generally indicate molecular flexibility in a wide range of systems.

The L-alanine zwitterion (ALAZW) itself serves traditionally as a good model of chiral systems of biological relevance, which can be treated at a relatively high level of approximation.[16,19−24] The zwitterionic form is not stable in vacuum and explicit or implicit solvent models have to be involved in a consistent modeling.[25] Most of observed vibrational transitions have been assigned in detail on the basis of a harmonic analysis of vibrational spectra, although some features in the spectra could not be explained in full.[16,26,27] Profound effect of solvation and conformer transitions in alanine was indicated by computations on explicit alanine−water clusters.[21] In this study, we take advantage of the latest efficient implementations of the polarizable continuum solvent models[2,28] and computations of ROA intensities implemented within the density functional theory (DFT)[29] facilitating modeling of the spectra for a large ensemble of conformers.

The ROA difference technique has been developed as an extension of the Raman spectroscopy allowing for chiral discrimination.[30] It proved to be particularly useful for structural studies of polar biopolymers (proteins, nucleic acids) in their natural aqueous environment.[31−34] ROA spectrum of ALAZW has been previously recorded using the incident circular polarization (ICP)[35,36] and dual circular polarization (DCP_I)[19] setup and fundamental transitions have been assigned to harmonic normal modes. The ROA DCP_I intensities are virtually identical to the ICP signal obtained on our instrument,[37,38] where, however, somewhat wider frequency region (100−1800 cm^{-1}) can be reached. We thus do not discuss in detail the normal mode assignment and concentrate on the characterization of the multidimensional molecular potential energy surface and its relation to the observed spectra

Method

All samples were purchased from Sigma and used without further purification. Backscattered Raman and incident circular

* To whom correspondence should be addressed. E-mail: baumruk@karlov.mff.cuni.cz (V.B.); bour@uochb.cas.cz (P.B.).
† Academy of Sciences.
‡ Charles University.

10.1021/jp060260o CCC: $33.50
Published on Web 03/17/2006

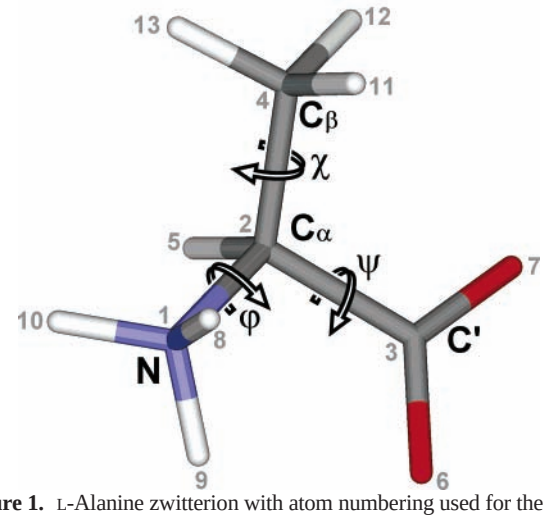

Figure 1. L-Alanine zwitterion with atom numbering used for the mode assignment.

polarization (ICP) ROA ALAZW solution spectra were recorded on our spectrometer described elsewhere.[37,38] All spectra were measured for nearly saturated solutions in doubly distilled deionized water at room temperature (~293 K), using the 514.5 nm excitation wavelength and spectral resolution of 6.5 cm^{-1}. The concentration of both L- and D-alanine was 1.6 M, and laser power at the sample was set to 430 mW. Additionally, spectra of four zwitterionic dipeptides of various rigidities were measured under the same setup, with a laser power at the sample of 570 mW. The concentrations/accumulation times were 2 M/6.3 h for Gly-Pro, 0.89 M/8.5 h for Pro-Gly, 1.33 M/7.5 h for Ala-Pro, and 0.23 M/27.5 h for Pro-Ala. Solvent signal was subtracted from the spectra, and minor baseline corrections were made.

To compare solution and solid-state Raman ALAZW signals, solution, crystalline, and glass spectra were recorded on an HR800 Raman microspectrometer (Horiba Jobin Yvon). Continuous Kiefer scanning mode was used with a 600 grooves/mm grating, a liquid-nitrogen-cooled CCD detector (1024 × 256 pixels), a spectral resolution of about 4 cm^{-1} (varying within the spectral range of frequencies recorded simultaneously), and 632.8 nm laser excitation wavelength. For crystalline ALAZW, a microscope objective of a moderate magnification (10×) was used to focus 4 mW of excitation laser power to a 2 μm diameter spot on the powder sample, and the spectrum was integrated for 120 s. Signal of the saturated solution 1.6 M L-alanine was detected in a macromode with 20 mW at the sample and an integration time of 10 min. The glass ALAZW form was prepared by deposition and evaporation of 4 μL of 0.01 mg/mL L-alanine solution on a standard drop-coating deposition Raman (DCDR) substrate SpectRIM (Tienta Sciences) consisting of a polished stainless steel plate coated with a thin hydrophobic Teflon layer.[39−41] The drop was allowed to dry for 20 min at room temperature, and the spectrum was collected with a 50× microscope objective, a 2 mW laser power, and an integration time of 32 min.

Gaussian[29] software was used for simulation of Raman and ROA intensities within the harmonic approximation. Three DFT functionals, B3P86, B3PW91, and B3LYP, and three standard basis sets of Gaussian, 6-31G**, 6-31++G**, and 6-311G**, were used, although not all the computations are discussed in detail. Rotational barriers for the CH_3, NH_3^+, and CO_2^- groups were estimated by one- (1D, for ψ, χ, φ) and two-dimensional (2D, for φ, ψ) scans along the dihedral angles defined in Figure 1, while the remaining coordinates were allowed to fully relax. The aqueous environment was accounted for by the COSMO continuum solvent model,[2,3] more specifically by its enhanced polarized continuum model (PCM) version that is in Gaussian referred to as CPCM.[29] Raman and ROA spectra were simulated with the B3LYP/6-31++G**/CPCM force field, HF/6-31++G**(vac) intensity tensors, and Lorenztian bands 6.5 cm^{-1} wide (full width at half-height). With the use of the energy scans, spectra of multiple conformers were averaged using the Boltzmann statistics for $T = 298$ K. For the 2D (φ, ψ) potential two-dimensional wave functions and probability distributions were calculated by solving the Schrödinger equation in nonorthogonal coordinates.[42,43] Numerical integration and a plane wave basis of 676 functions were used; the final probability distribution was obtained by Boltzmann weighting of all state probabilities.

TABLE 1: Computed Geometrical Parameters of ALAZW

angle[a]	B3LYP	B3P86	P3BW91	ref 24
Equilibrium Geometry				
$\psi(CO_2^-)$	−15	5	8.1	0
$\varphi(NH_3^+)$	40	110	105	30
$\chi(CH_3)$	178	178	178	180
Ground-State Average (2D φ, ψ scan)[b]				
$\psi(CO_2^-)$	−13(7)	4(7)		
$\varphi(NH_3^+)$	47(17)	107(15)		
Boltzmann Averaging for 298 K[b]				
$\psi(CO_2^-)$	−4(17)	−2(16)		
$\varphi(NH_3^+)$	62(31)	119(34)		

[a] In deg, defined in Figure 1. [b] The rms deviations are given in parentheses.

Results

L-Alanine Torsional Motions. Similarly as done for ALAZW in the gas phase previously,[24] we mapped the molecular potential

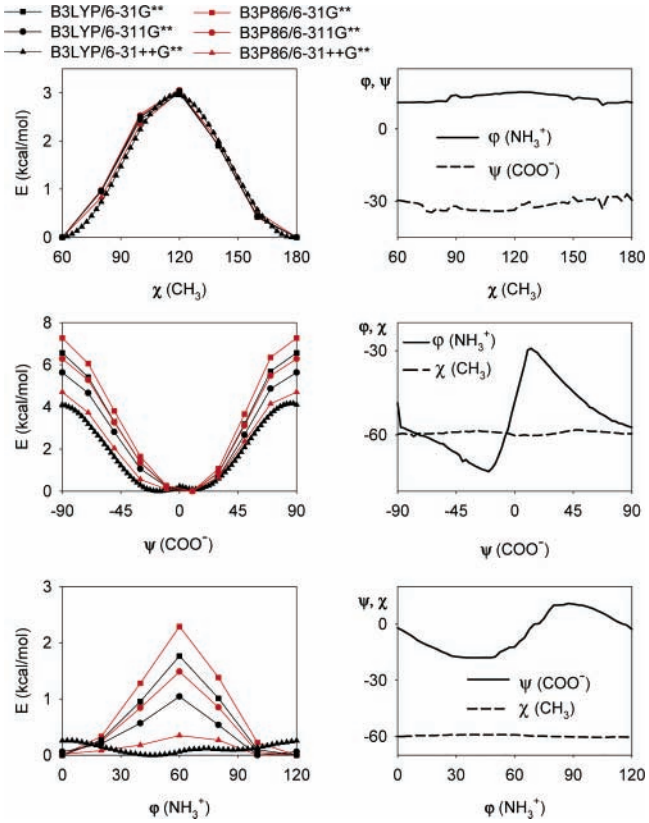

Figure 2. Dependencies of molecular energy (E, left) and dihedral angles (right) on the angles φ, ψ, and χ (in deg, defined in Figure 1). The remaining coordinates in the one-dimensional scans were allowed to fully relax.

TABLE 2: Calculated (6-31++G/CPCM) and Experimental ALAZW Fundamental Frequencies (ω (cm^{-1})), Observed Bandwidths (Δ), and Normal Mode Assignment**

			solution		crystalline powder		gellike glass		
mode	ω_{B3LYP}	ω_{B3P86}	ω	Δ^a	ω	Δ^a	ω	Δ^a	SAIC(PED)[b]
1	35	39							33(78)
2[c]	88	112			139, 159	16, 8			32(62) 31(15)
3[c]	228	236			193, 219	16, 17			31(70) 32(22)
4	264	260	279	42	264, 282	10, 23	278	23	26(53) 31(21)
5	321	324	338	57	323	21	350	46	26(32) 25(26) 31(25)
6	391	394	407	42	398	22	411	39	27(40) 31(32)
7	506	518	529	26	477, 531	14, 12	533	29	29(43)
8	588	608	608, 645	70, 40	650	16	597, 641	41, 54	11(24) 28(22)
9	759	764	775	19	771	10	774	15	30(30) 31(25)
10	825	836	848	16	851	7	849	18	28(20) 31(17)
11	886	897	922	16	920	11	922	22	10(30) 11(26) 21(15)
12	951	968	1003	28	1011	9	981	21	17(26) 16(24) 21(19) 12(18)
13	976	988	(1003)	(28)	1019	8	1003	24	22(32) 16(22)
14	1090	1094	1113	17	1113	7	1113	18	17(16) 10(14)
15	1116	1125	1138	35	1146	12	1131	44	22(24) 26(20)
16	1195	1200	1215	32	1236	11	1207	30	21(19) 16(17)
17	1316	1308	1303	16	1305	8	1302	27	24(49) 8(17)
18	1366	1366	1354	19	1359	7	1350	27	23(50)
19	1383	1387	1378	11	1377	7	1374	23	8(34) 18(16)
20	1415	1395	1414	18	1408, 1416	8, 10	1413	29	18(67)
21	1455	1426	(1414)	(18)	1461	6	(1413)	29	13(74)
22	1490	1486	1457	11	1482	5	1459	29	20(40) 19(38)
23	1494	1489	1467	11	1499	16	(1459)	29	19(42) 20(37)
24	1580	1585	1597	55	1546, 1596	18, 11	1608	58	14(69)
25	1626	1626	1630	59	1621	16	1655	48	15(72) 9(16)
26	1633	1676	(1630)	(59)	1648	9	(1655)	48	9(68)
27[c]	3015	3034	2873	20	2877	12	2854	32	7(96)
28[c]	3041	3056	2895	23	2890	16	2887	35	5(49) 4(37)
29[c]	3105	3110	2927	38	2933	33	2922	50	4(55) 5(42)
30[c]	3152	3131	2951	17	(2933)	33	2944	25	6(87)
31[c]	3261	3172	2972	29	2961, 2967	16, 9	2980	42	1(67) 3(18) 2(15)
32[c]	3321	3344	2994	24	2987	9	3002	31	2(52) 1(32) 3(16)
33[c]	3349	3395	3012	28	3001	5	(3002)	31	3(65) 2(32)

[a] The widths (cm^{-1}) were obtained by fitting with mixed Gaussian−Lorentzian peaks. [b] Potential energy distributions (PED, in %) based on the B3LYP computation. Values bigger than 15% are listed; the SAIC coordinates are defined in Table 3. [c] Assignments of fundamentals 2−3 and anharmonic N−H and C−H stretching modes (nos. 27−33) should be considered speculative.

energy surface (PES) as a function of the angles defined in Figure 1 with the CPCM water medium model. Equilibrium geometry parameters are listed in Table 1. Clearly, especially the values of the ψ, φ angles are quite dependent on the approximation. Moreover, while probing the PES more thoroughly, we found a rather different behavior of the three rotating groups, which can be documented by the one-dimensional scans in Figure 2. The rotation of the CH_3 group represents the simplest case. First, it can be associated with a well-defined harmonic normal mode coordinate, with computed harmonic frequency of about 228 cm^{-1} (refs 19, 16, Table 3). Also, this motion is well-separated from the other two rotations, as can be estimated from their dependence on the χ angle at the upper right corner of Figure 2. The corresponding rotational barrier of about 3 kcal/mol is predicted consistently by all the six levels of approximation used. Finally, solid-state spectra (given below) will suggest that the fundamental transition of this mode provides a

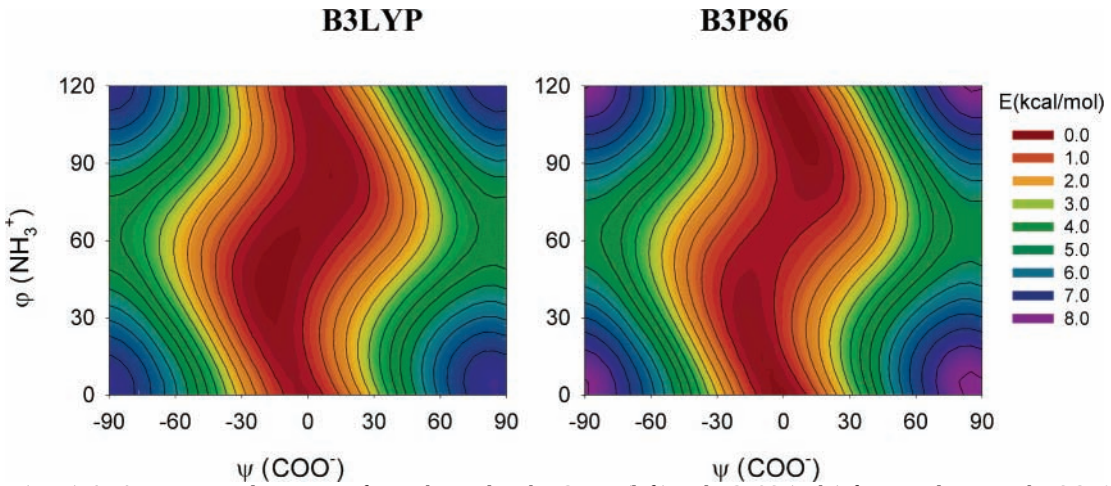

Figure 3. 2D (ψ, φ) ALAZW potential energy surfaces obtained with B3LYP (left) and B3P86 (right) functionals, using the 6-31++G** basis and CPCM solvent correction. The equipotential lines are separated by 0.5 kcal/mol.

TABLE 3: Definitions of Symmetry-Adapted Internal Coordinates (SAIC) of ALAZW Used in Table 2[a]

SAIC	definition	SAIC	definition
1 υ (NH)	$R_{1,8}$	18 d_s (CH_3)	$B_{11,4,12} + B_{11,4,13} + B_{12,4,13} - B_{13,4,2} - B_{12,4,2} - B_{11,4,2}$
2 υ (NH)	$R_{1,9}$	19 d_a (CH_3)	$2B_{11,4,12} - B_{11,4,13} - B_{12,4,13}$
3 υ (NH)	$R_{1,10}$	20 d_a (CH_3)	$B_{11,4,13} - B_{12,4,13}$
4 υ ($C_\beta H$)	$R_{4,11}$	21 r (CH_3)	$2B_{13,4,2} - B_{12,4,2} - B_{11,4,2}$
5 υ ($C_\beta H$)	$R_{4,12}$	22 r (CH_3)	$B_{12,4,2} - B_{11,4,2}$
6 υ ($C_\beta H$)	$R_{4,13}$	23 r ($C_B H$)	$2B_{5,2,1} - B_{5,2,3} - B_{5,2,4}$
7 υ ($C_\alpha H$)	$R_{2,5}$	24 r ($C_B H$)	$B_{5,2,3} - B_{5,2,4}$
8 υ_s (CO_2)	$R_{3,6} + R_{3,7}$	25 d (NC_BC')	$4B_{1,2,3} + B_{1,2,4} + B_{3,2,4}$
9 υ_a (CO_2)	$R_{3,6}$ $R_{3,7}$	26 d ($C_\beta C_B C'$)	$B_{1,2,3} + 4B_{1,2,4} + B_{3,2,4}$
10 υ (NC_α)	$R_{1,2}$	27 d (NC_BC_β)	$B_{1,2,3} + B_{1,2,4} + 4B_{3,2,4}$
11 υ ($C_\alpha C'$)	$R_{2,3}$	28 d_s (CO_2)	$2B_{6,3,7} - B_{2,3,6} - B_{2,3,7}$
12 υ ($C_\alpha C_\beta$)	$R_{2,4}$	29 r (CO_2)	$B_{2,3,6} - B_{2,3,7}$
13 d_s (NH_3)	$B_{8,1,9} + B_{8,1,10} + B_{9,1,10} - B_{9,1,2} - B_{10,1,2} - B_{8,1,2}$	30 t (CO_2)	$D_{2,3,6,7}$
14 d_a (NH_3)	$2B_{8,1,9} - B_{8,1,10} - B_{9,1,10}$	31 t ($N-C_B$)	$D_{8,1,2,3}$
15 d_a (NH_3)	$B_{8,1,10} - B_{9,1,10}$	32 t ($C'-C_B$)	$D_{1,2,3,6}$
16 r (NH_3)	$2B_{9,1,2} - B_{10,1,2} - B_{8,1,2}$	33 t ($C_\beta-C_B$)	$D_{1,2,4,11}$
17 r (NH_3)	$B_{10,1,2} - B_{8,1,2}$		

[a] Used abbreviations: υ, stretch (a-locally asymmetric, s-symmetric); d, deformation; r, rocking; t, torsion; for distances, bond and dihedral angles symbols R, B, and D are used, respectively; atom numbering defined in Figure 1.

strong distinct Raman signal, although the signal is not measurable in the solution spectra.

On the other hand, harmonic frequencies corresponding to the rotations of the CO_2^- and NH_3^+ groups lie below 100 cm^{-1}, and the two normal mode coordinates are mixed. Additionally, frequencies of these low-energy modes are calculated with a big relative error. This is a general problem with ab initio Hessians of finite accuracy and has been described previously.[44] The one-dimensional energy dependencies plotted in Figure 2 provide shallow potential wells/plateaus for the minima. For the rotational barrier of CO_2^- the computations seem to converge to the value of about 4 kcal/mol obtained for the best basis set (6-31++G**), while for NH_3^+ the barrier is lower and practically disappears for the best basis. The BPW91/6-31++G** and B3LYP/6-31++G** computations provide different equilibrium φ angles of 105° and 40°, respectively. Additionally, the two rotational motions are strongly coupled, as can be estimated from the dependencies plotted at the right-hand side of Figure 2. All the barriers appear somewhat smaller than those obtained for vacuum.[24]

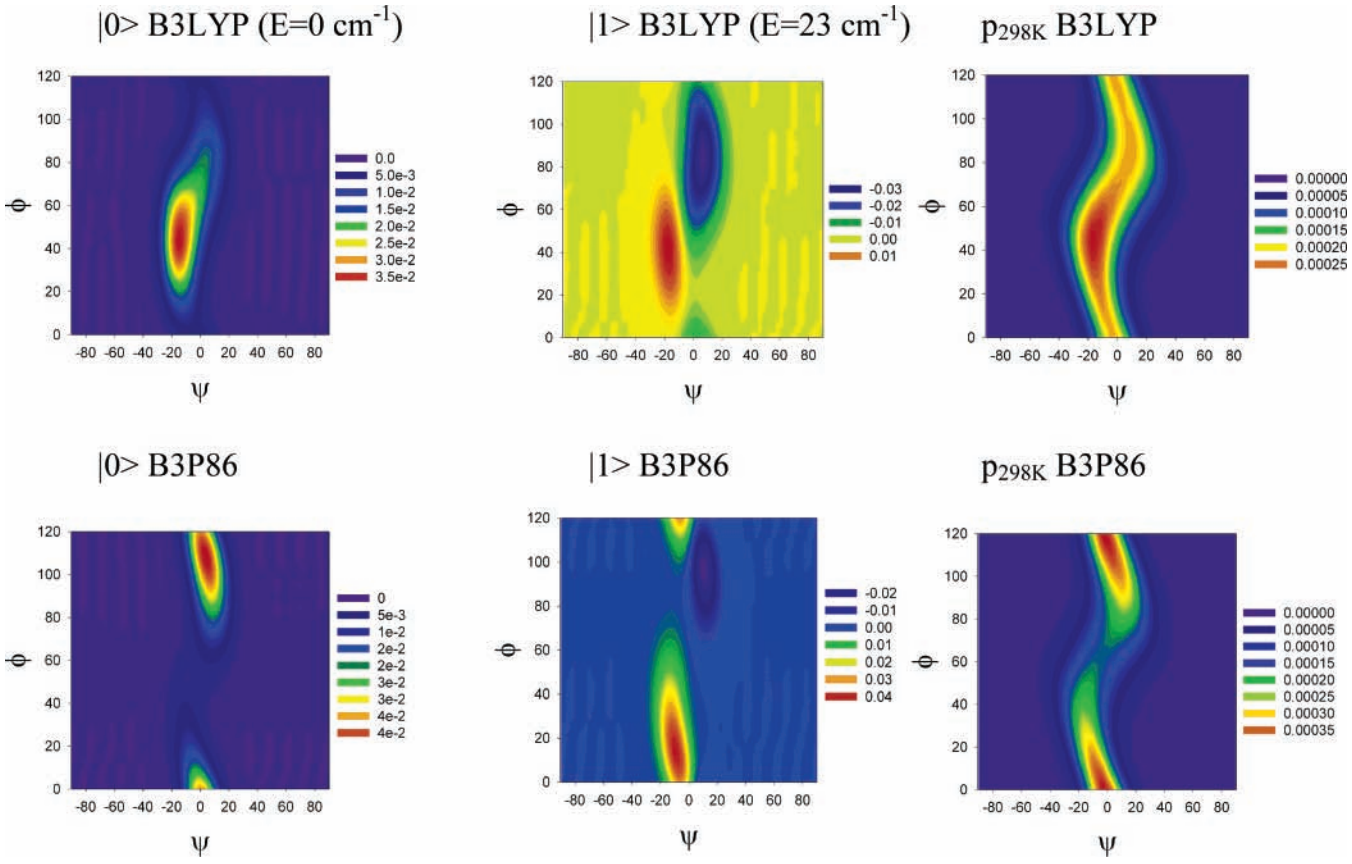

Figure 4. Wave functions of the ground (|0>) and first (|1>) excited vibrational states, and probability distributions obtained by Boltzmann averaging at 298 K, for the potential energy surfaces given in Figure 3. Results obtained for the B3LYP and B3P86 functionals are plotted at the top and bottom, respectively.

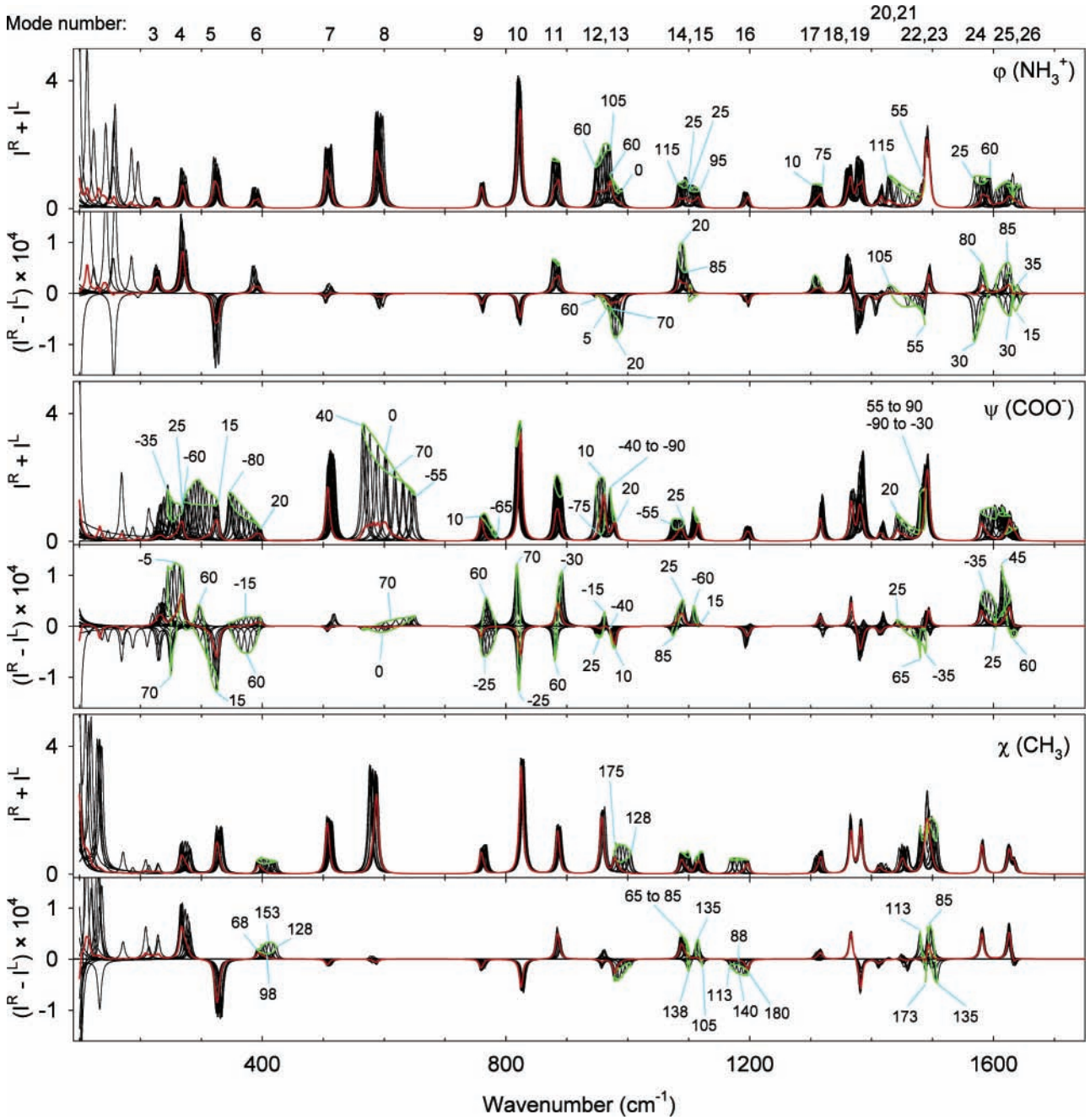

Figure 5. Simulated dependence of Raman and ROA intensities of L-ALAZW on the rotations of the NH_3^+, CO_2^-, and CH_3 groups. Spectra obtained by the Boltzmann averaging are plotted in red. For easier orientation, green lines connect peak extremes and selected torsion angle values are indicated within spectra boxes; mode numbers are assigned at the top.

Because of the coupling, the full 2D PES maps displayed in Figure 3 provide a better basis for understanding of the molecular motion. Here surfaces obtained by the B3LYP and B3P86 functionals are compared, the latter giving approximately the same minima as BPW91 (see also Table 1). Despite the different location of the minima, the two computations provide similar shallow sinusoidal "valleys" controlled by correlated rotations of the CO_2^- and NH_3^+ groups. Large deviations from the equilibrium structure are possible, as can be estimated from the wave functions and probability distributions plotted in Figure 4. At 298 K the B3LYP computation predicts almost a free rotation of the NH_3^+ group, while CO_2^- moves much less (see the root-mean-square (rms) deviations of about 31° and 17°, respectively, listed at the lower part of Table 1).

Spectral Peak Broadenings. The motions of the three rotating groups influence fundamental vibrations of the remaining normal mode coordinates differently. This can be documented in Figure 5 where the Raman and ROA intensities are simulated for different rotamers. To separate the motions by preventing rotation coupling, the CO_2^- conformation was fixed in its equilibrium position during the NH_3^+ rotation, and vice versa. We can thus see, for example, that the sole NH_3^+ rotation does not significantly change peak positions within 250−890 cm^{-1}, although it can significantly modulate the Raman and ROA intensities in that region. In the same frequency interval, the CO_2^- rotation is reflected by changes of both peak positions and their intensities. The band centered around 588 cm^{-1} (CH_3 rocking, see Tables 2 and 3) appears particularly sensitive to the CO_2^- movement and changes the position within ∼100 cm^{-1} during the rotation. Higher-frequency peaks (∼900−1680 cm^{-1}) react qualitatively similarly to the NH_3^+ and CO_2^- rotations. By contrast, the rotation of the CH_3 group has a relatively minor

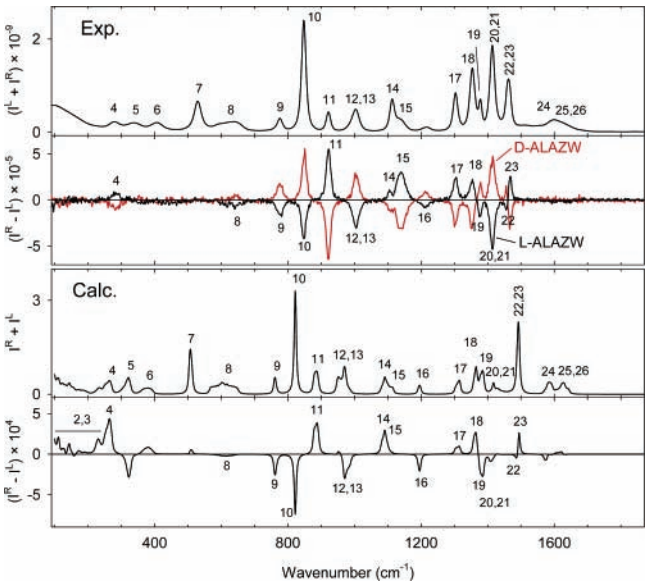

Figure 6. Comparison of experimental Raman and ROA ICP spectra of ALAZW in solution with simulations obtained using the Boltzmann average over ψ, φ rotamers. Experimental ROA spectra of both enantiomers are plotted, while the L-form was simulated only.

effect on the spectra. Interestingly, however, it often affects bands relatively unperturbed by the movement of the charged groups. For example, the band at 1200 cm^{-1} is affected almost solely by the CH_3 rotation, changing its position within ~30 cm^{-1}. More importantly, ROA signs of about half of the total number of the bands can be reversed by rotations involving the three χ, φ, ψ angles, a phenomenon perhaps rather surprising for such a simple molecule as ALAZW. Nevertheless, similar sensitivity was observed lately for another form of molecular chirality of small molecules, the optical rotation.[23]

Despite the different equilibrium geometries, we obtained quite similar Raman and ROA-averaged spectra with the B3LYP and B3P86 functionals. Therefore, only the B3LYP results are discussed further. The spectra nicely correspond to the experiment, as can be seen in Figure 6. Particularly, for the Raman signal, the broader relative widths of peaks corresponding to normal mode nos. 4−6, 8, and 24−26 can be explained by the molecular flexibility (cf., Figures 5 and 6). Overall, the experimental line widths, however, are still slightly wider, which can be attributed to a dynamical influence of the solvent, not included in the static CPCM model. ROA intensities of peaks most affected by the broadening are rather low. Especially, the experimental signal for modes 4−8 and 24−26 is on the brink of the detection limits, which qualitatively corresponds to the simulation. The predicted strong negative intensity at 320 cm^{-1} was not observed, but the overall positive signal at this region is consistent. Unfortunately, our simulation is rather deficient in the C−H, N−H bending region (1415−1500 cm^{-1}) where perhaps anharmonic interactions perturb the spectra.

Flexibility of ALAZW in Different States. Previously, for molecules in the vicinity of surfaces,[18] it was suggested that rotations of some flexible groups may be hindered. We observed an analogous phenomenon while comparing Raman intensities obtained for glass, solution, and a crystalline powder sample as plotted in Figure 7. Typically, the crystalline-state spectra provide sharper bands, and they can be better identified with simulation for the equilibrium structure (lowest trace in Figure 7), while the averaging (Figure 6) is desirable for correct interpretation of the solution signal. For example, the fundamental band no. 8 is much narrower in the crystalline-state

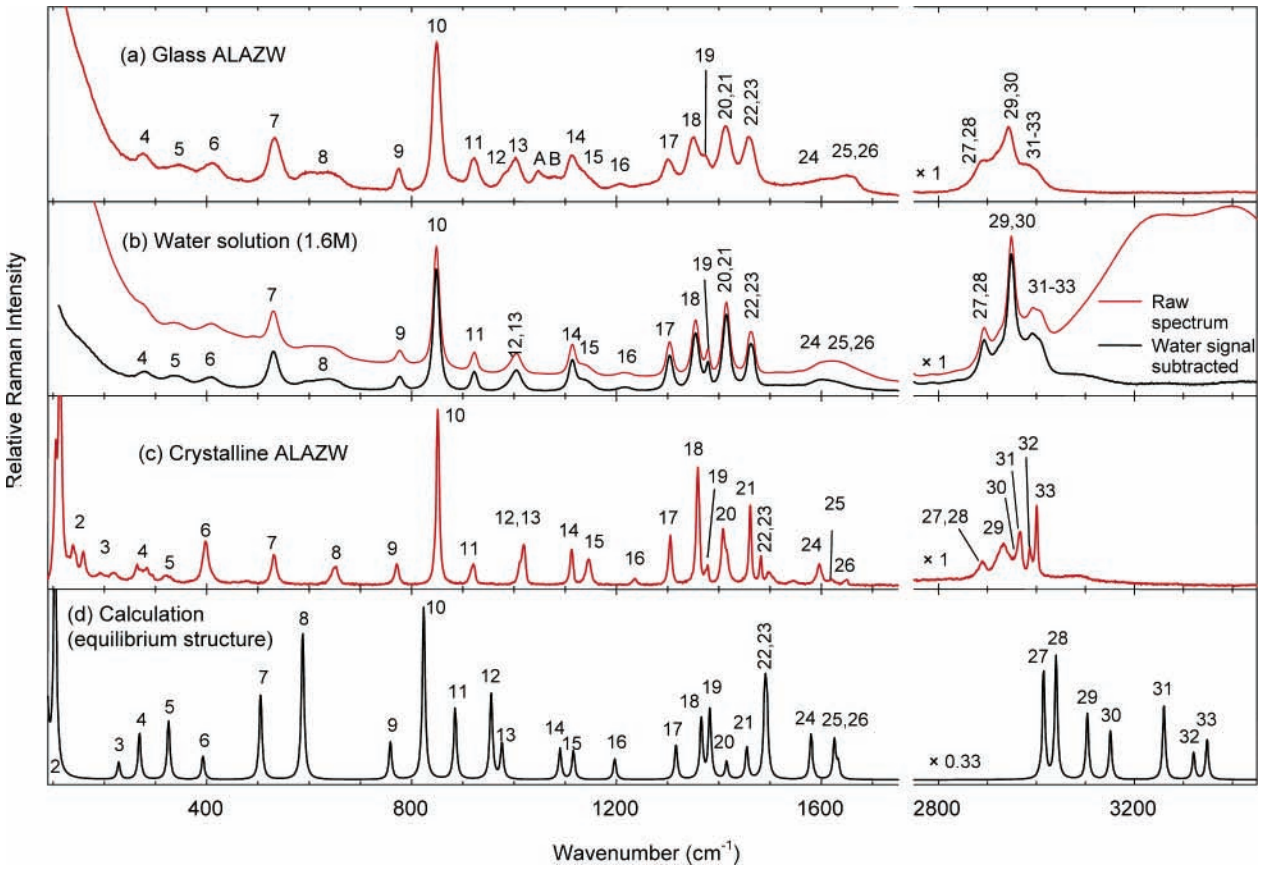

Figure 7. Comparison of experimental Raman spectra of ALAZW in (a) glass, (b) 1.6 M aqueous solution, and (c) crystalline sample with (d) spectrum simulated (B3LYP/6-31++G**/CPCM) for the equilibrium geometry.

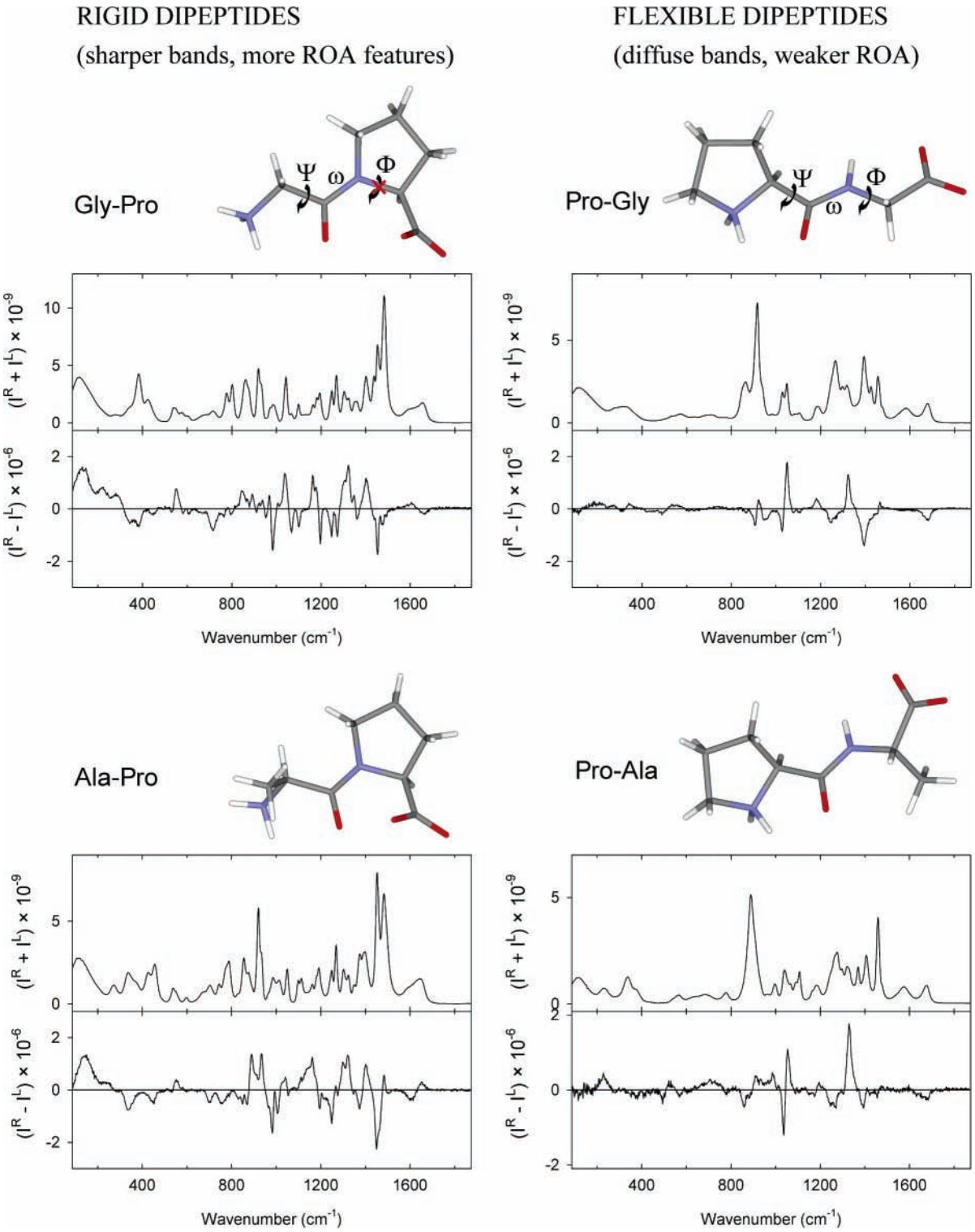

Figure 8. Experimental Raman and ROA spectra of four zwitterionic dipeptides of various rigidities.

spectrum, most probably because of the freezing of the CO_2^- rotation. Similarly, Raman bands of the modes 24−26 can be resolved here. Note, however, that the single conformer computation for an isolated molecule may not be entirely relevant for the simulation of the crystal spectrum, which is perhaps indicated by the relative intensity disagreement, namely, for the bands within 200−400 cm^{-1}. Microcrystal spectra were also somewhat sensitive to the crystal orientation, detailed analysis of which goes beyond the aims of present work. However, the signal of the CH_3 rotation (mode no. 3), probably not significantly affected by the crystal forces, can be clearly identified in the crystalline-state spectra. In contrast, the glass spectrum is much closer to that obtained in the solution. Supposedly, during the gel/glass formation, a random distribution of the φ, ψ, χ angles in ALAZW was conserved, similar to that in the solution. Note that water is almost entirely absent in the glass phase, as can be estimated from the lack of the signal of the O−H stretching within 3100−3600 cm^{-1}. We cannot explain the specific glass bands at 1047(18) and 1077-(63) cm^{-1} (A, B in Figure 7, peak widths are in parentheses). Otherwise the glass peak frequencies almost coincide with the solution values, and peak widths (both summarized in Table 2)

are mostly only slightly bigger, except of some lowest-energy bands (nos. 4, 5, 6, and 9), narrower in the glass.

Qualitative Comparison of Spectra of Rigid and Flexible Molecules. We can thus conclude that ALAZW molecular flexibility can significantly modify Raman and ROA spectral intensities, band positions, and, in an extreme case, the ROA signs. Additionally, the spectra of bigger zwitterionic dipeptides presented in Figure 8 suggest that the potential of the method to monitor molecular flexibility is retained also for larger systems and that the broadening of spectral lines is crucial for spectral interpretation. Indeed, for the relatively rigid Gly-Pro and Ala-Pro zwitterionic peptides, where only one (ψ) main chain torsion angle moves freely, the Raman and ROA spectra presented on the left-hand side of Figure 8 exhibit the "rigid features" consisting in sharp Raman bands and relatively intense ROA signal within 200−750 cm^{-1}. On the other hand, the spectra of presumably more flexible Pro-Gly and Pro-Ala where two main chain angles (ψ, φ) can move (plotted at the right-hand side of Figure 8) are, at least visually, quite different and more in line with the "flexible" ALAZW spectrum (broader bands, small signal in the lowest-frequency region). We can additionally speculate that the terminal CO_2^- group (largely perturbing the bands for ALAZW, see Figure 5) in the flexible Pro-Gly and Pro-Ala molecules rotates more because the coupling with the proline ring motion is removed.

Conclusions

For ALAZW we have seen that the analysis of the Raman and ROA spectra in solution is in agreement with the molecular potential energy surface obtained ab initio. Motions of different molecular parts selectively broaden different spectral bands. The spectrum of the crystalline sample was consistent with a one-geometry model, while simulations for the solution or glass states required conformer averaging. Thus, the combination of Raman spectroscopy and ab initio analysis may not only reveal an average molecular structure but also map real geometric dispersion. As indicated for the bigger dipeptides, the conformational broadening should be always taken into account for spectra of flexible systems. If seen from another perspective, the Raman and ROA spectroscopies thus provide a relatively simple means for monitoring of basic molecular motions in peptides.

Acknowledgment. This work was supported by the Grant Agency (Grant No. 203/06/0420) and by the Ministry of Education (MSM 0021620835) of the Czech Republic.

References and Notes

(1) *The Encyclopedia of Computational Chemistry*; Schleyer, P. R., Allinger, N. L., Clark, T., Gasteiger, J., Kollman, P. A., Schaefer, H. F., III, Schreiner, P. R., Eds.; John Wiley & Sons: Chichester, U.K., 1998.

(2) Klamt, A.; Schuurmann, G. *J. Chem. Soc., Perkin Trans.* **1993**, *2*, 799.

(3) Klamt, A. *J. Phys. Chem.* **1995**, *99*, 2224.

(4) Pecul, M.; Marchesan, D.; Ruud, K. *J. Chem. Phys.* **2005**, *122*, 024106.

(5) Cammi, R.; Corni, S.; Mennucci, B.; Tomasi, J. *J. Chem. Phys.* **2005**, *122*, 104513.

(6) Caricato, M.; Ingrosso, F.; Mennucci, B.; Tomasi, J. *J. Chem. Phys.* **2005**, *122*, 154501.

(7) Tu, A. T. *Raman Spectroscopy in Biology*; Wiley: New York, 1982.

(8) Yang, S.; Cho, M. *J. Chem. Phys.* **2005**, *123*, 134503.

(9) Ham, S.; Kim, J. H.; Kochan, L.; Cho, M. *J. Chem. Phys.* **2003**, *118*, 3491.

(10) Asher, S. A.; Ianoul, A.; Mix, G.; Boyden, M. N.; Karnoup, A.; Diem, M.; Schweitzer-Stenner, R. *J. Am. Chem. Soc.* **2001**, *123*, 11775.

(11) Bouř, P.; Michalík, d.; Kapitán, J. *J. Chem. Phys.* **2005**, *122*, 144501.

(12) Bouř, P.; Keiderling, T. A. *J. Phys. Chem. B* **2005**, *109*, 23687.

(13) Ashvar, C. S.; Devlin, F. J.; Stephens, P. J. *J. Am. Chem. Soc.* **2000**, *121*, 2836.

(14) Aamouche, A.; Devlin, F. J.; Stephens, P. J. *J. Am. Chem. Soc.* **2000**, *122*, 7358.

(15) Jalkanen, K. J.; Nieminen, R. M.; Knapp-Mohammady, M.; Suhai, S. *Int. J. Quantum Chem.* **2003**, *92*, 239.

(16) Abdali, S.; Jalkanen, K. J.; Bohr, H.; Suhai, S.; Nieminen, R. M. *Chem. Phys.* **2002**, *282*, 219.

(17) Jalkanen, K. J.; Elstner, M.; Suhai, S. *J. Mol. Struct. (THEOCHEM)* **2004**, *675*, 61.

(18) Netti, C.; Lincoln, J. R. *Microsc. Microanal.* **2005**, *16*, 17.

(19) Yu, G. S.; Freedman, T. B.; Nafie, L. A.; Deng, Z. Y.; Polavarapu, P. L. *J. Phys. Chem.* **1995**, *99*, 835.

(20) Frimand, K.; Bohr, H.; Jalkanen, K. J.; Suhai, S. *Chem. Phys.* **2000**, *255*, 165.

(21) Tajkhorshid, E.; Jalkanen, K. J.; Suhai, S. *J. Phys. Chem. B* **1998**, *102*, 5899.

(22) Park, S. W.; Ahn, D. S.; Lee, S. *Chem. Phys. Lett.* **2003**, *371*, 74.

(23) Pecul, M.; Ruud, K.; Rizzo, A.; Helgaker, T. *J. Phys. Chem. A* **2004**, *108*, 4269.

(24) Selvarengan, P.; Kolandaivel, P. *J. Mol. Struct. (THEOCHEM)* **2004**, *671*, 77.

(25) Ahn, D. S.; Park, S. W.; Jeon, I. S.; Lee, M. K.; Kim, N. H.; Han, Y. H.; Lee, S. *J. Phys. Chem. B* **2003**, *107*, 14109.

(26) Diem, M. *J. Am. Chem. Soc.* **1988**, *110*, 6967.

(27) Gontrani, L.; Mennucci, B.; Tomasi, J. *J. Mol. Struct. (THEOCHEM)* **2000**, *500*, 113.

(28) Cossi, M.; Barone, V.; Cammi, R.; Tomasi, J. *Chem. Phys. Lett.* **1996**, *255*, 327.

(29) Frisch, M. J.; Trucks, G. W.; Schlegel, H. B.; Scuseria, G. E.; Robb, M. A.; Cheeseman, J. R.; Montgomery, J. A., Jr.; Vreven, T.; Kudin, K. N.; Burant, J. C.; Millam, J. M.; Iyengar, S. S.; Tomasi, J.; Barone, V.; Mennucci, B.; Cossi, M.; Scalmani, G.; Rega, N.; Petersson, G. A.; Nakatsuji, H.; Hada, M.; Ehara, M.; Toyota, K.; Fukuda, R.; Hasegawa, J.; Ishida, M.; Nakajima, T.; Honda, Y.; Kitao, O.; Nakai, H.; Klene, M.; Li, X.; Knox, J. E.; Hratchian, H. P.; Cross, J. B.; Bakken, V.; Adamo, C.; Jaramillo, J.; Gomperts, R.; Stratmann, R. E.; Yazyev, O.; Austin, A. J.; Cammi, R.; Pomelli, C.; Ochterski, J. W.; Ayala, P. Y.; Morokuma, K.; Voth, G. A.; Salvador, P.; Dannenberg, J. J.; Zakrzewski, V. G.; Dapprich, S.; Daniels, A. D.; Strain, M. C.; Farkas, O.; Malick, D. K.; Rabuck, A. D.; Raghavachari, K.; Foresman, J. B.; Ortiz, J. V.; Cui, Q.; Baboul, A. G.; Clifford, S.; Cioslowski, J.; Stefanov, B. B.; Liu, G.; Liashenko, A.; Piskorz, P.; Komaromi, I.; Martin, R. L.; Fox, D. J.; Keith, T.; Al-Laham, M. A.; Peng, C. Y.; Nanayakkara, A.; Challacombe, M.; Gill, P. M. W.; Johnson, B.; Chen, W.; Wong, M. W.; Gonzalez, C.; Pople, J. A. *Gaussian 03*, revision C.02; Gaussian, Inc.: Wallingford, CT, 2004.

(30) Barron, L. D. *Molecular Light Scattering and Optical Activity*; Cambridge University Press: Cambridge, 2004.

(31) Barron, L. D.; Hecht, L.; Bell, A. D. Vibrational Raman Optical Activity of Biomolecules. In *Circular Dichroism and the Conformational Analysis of Biomolecules*; Fasman, G. D., Ed.; Plenum: New York, 1996; p 653.

(32) Blanch, E. W.; Morozova-Roche, L. A.; Cochran, D. A. E.; Doig, A. J.; Hecht, L.; Barron, L. D. *J. Mol. Biol.* **2000**, *301*, 553.

(33) Blanch, E. W.; Hecht, L.; Barron, L. D. *Methods* **2003**, *29*, 196.

(34) Yu, G. S.; Che, D. P.; Freedman, T. B.; Nafie, L. A. *Biospectroscopy* **1995**, *1*, 113.

(35) Barron, L. D.; Gargaro, A. R.; Hecht, L.; Polavarapu, P. L. *Spectrochim. Acta, Part A* **1991**, *47*, 1001.

(36) Barron, L. D.; Gargaro, A. R.; Hecht, L.; Polavarapu, P. L. *Spectrochim. Acta, Part A* **1992**, *48*, 261.

(37) Kapitán, J.; Baumruk, V.; Gut, V.; Hlaváček, J.; Dlouhá, H.; Urbanová, M.; Wunsch, E.; Maloň, P. *Collect. Czech. Chem. Commun.* **2005**, *70*, 403.

(38) Bouř, P.; Baumruk, V.; Hanzlíková, J. *Collect. Czech. Chem. Commun.* **1997**, *62*, 1384.

(39) Deegan, R. D.; Bakajin, O.; Dupont, T. F.; Huber, G.; Nagel, S. R.; Witten, T. A. *Nature* **1997**, *389*, 827.

(40) Zhang, D.; Xie, Y.; Mrozek, M. F.; Ortiz, C.; Davisson, V. J.; Ben-Amotz, D. *Anal. Chem.* **2003**, *75*, 5703.

(41) Zhang, D.; Mrozek, M. F.; Xie, Y.; Ben-Amotz, D. *Appl. Spectrosc.* **2004**, *58*, 929.

(42) Čejchan, A.; Špirko, V. *J. Mol. Spectrosc.* **2003**, *217*, 142.

(43) Podolsky, B. *Phys. Rev.* **1928**, *32*, 812.

(44) Montgomery, J. A.; Frisch, M. J.; Ochterski, J. W.; Petersson, G. S. *J. Chem. Phys.* **1999**, *110*, 2822.